Jay T. Miller[1]
Department of Civil and Environmental Engineering, Massachusetts Institute of Technology, Cambridge, MA 02139

Connor G. Mulcahy
Department of Mechanical Engineering, Massachusetts Institute of Technology, Cambridge, MA 02139

Jahir Pabon
Schlumberger-Doll Research, Cambridge, MA 02139

Nathan Wicks
Schlumberger-Doll Research, Cambridge, MA 02139

Pedro M. Reis[2]
Department of Mechanical Engineering, Department of Civil and Environmental Engineering, Massachusetts Institute of Technology, Cambridge, MA 02139
e-mail: preis@mit.edu

Extending the Reach of a Rod Injected Into a Cylinder Through Distributed Vibration

We present results of an experimental investigation of a new mechanism for extending the reach of an elastic rod injected into a horizontal cylindrical constraint, prior to the onset of helical buckling. This is accomplished through distributed, vertical vibration of the constraint during injection. A model system is developed that allows us to quantify the critical loads and resulting length scales of the buckling configurations, while providing direct access to the buckling process through digital imaging. In the static case (no vibration), we vary the radial size of the cylindrical constraint and find that our experimental results are in good agreement with existing predictions on the critical injection force and length of injected rod for helical buckling. When vertical vibration is introduced, reach can be extended by up to a factor of four, when compared to the static case. The injection speed (below a critical value that we uncover), as well as the amplitude and frequency of vibration, are studied systematically and found to have an effect on the extent of improvement attained.
[DOI: 10.1115/1.4029251]

1 Introduction

The insertion of a slender rodlike structure into a cylindrical constraint can lead to buckled configurations that may eventually jam, or *lock-up*, the system and prevent further injection [1]. This process arises in a variety of natural and engineering systems, ranging from deoxyribonucleic acid and nanorods [2], to vascular catheters [3], and coiled tubing operations in the oilfield [4]. In particular, for the latter example at the kilometer scale, the axial force that drives buckling typically builds up due to the frictional interaction between the filamentary structure and the surface of the pipe [5] or collision with an obstruction [6].

Earlier studies on the constrained buckling of rods focused on the case of compression of a fixed length of rod inside of a frictionless cylinder [7–10] and the effect of friction was considered subsequently [11–14]. Suryanarayana and McCann [15] introduced transverse vibrations in their experiments, which they found could be used to reduce frictional effects, even though the process was not explored systematically. More recently, the lock-up of a frictional rod injected into a cylinder has been studied in the context of coiled tubing operations in horizontal wells [16,17]. Coiled tubing is a continuous length of steel pipe that can be inserted continuously and efficiently (compared to drill pipe, which is added in discrete 30-foot-long sections) into a producing wellbore for a variety of interventions including clearing produced sand, removing near-wellbore damage, or data logging [18,19]. While current drilling technologies have enabled drilling wells with horizontal sections over 11 km long [20], coiled tubing is unable to access the total depth of such wells [21]. Efforts in delaying lock-up, also known as *reach extension*, studied in the literature can be characterized as either *passive* methods (e.g., changing the coiled tubing's material [17], diameter [22], removing imperfections [23], or using friction reducing fluid [24]), or *active* methods (e.g., employing a device such as a tractor [25] or vibrator [26]). Predictively understanding the mechanisms underlying lock-up and devising ways to delay its onset is a challenging endeavor given the nature of the nonlinearities involved, both at the level of geometry of the rod [27] and the contact with the constraint.

Here, we experimentally explore a mechanism for delaying the helical buckling process of a rod injected into a horizontal cylindrical constraint. The frictional contacts between the rod and pipe during insertion are destabilized by vertical transverse vibrations of the constraining pipe. This results in a significant extension of reach by as much as a factor of four, when compared to the static case (no vibration). This mechanism involves the dynamical response of the buckled configurations of the rod and is strongly affected by the injection speed of the rod, as well as the frequency and amplitude of the vibration. Our findings suggest a possible mitigation method for delaying lock-up in coiled tubing operations in extended reach wells and provide design guidelines in terms of injection speed and vibration parameters.

Our paper is organized as follows: In Sec. 2, we present our experimental model system for injecting a rod into a horizontal cylindrical constraint with a distributed shaker system. The experiment is first run without vertical vibration in Sec. 3, with the results compared to existing theoretical predictions. In Sec. 4, we consider experiments with vertical vibration, where the results are normalized by the corresponding static values to quantify the relative improvements in reach. Conclusions are given in Sec. 5.

2 Experimental Setup

In our benchtop precision model experiments, we rescale the original problem of the lock-up of coiled tubing in horizontal wellbores at the kilometer scale for systematic exploration. A slender elastomeric rod is injected into a horizontal pipe, which can be either *static* or *vibrated vertically*. This analog system is studied in a laboratory setting, with the emphasis of exploring mechanisms to extend reach.

In Fig. 1 (insets: I–V), we present representative photographs (side view) of the *static case*, as the length of injected rod, l, is progressively increased at a constant injection velocity, v. Initially, straight rod (Fig. 1, I) first buckles into a sinusoidal mode

[1]Present address: Schlumberger-Doll Research, Cambridge, MA 02139.
[2]Corresponding author.

Contributed by the Applied Mechanics of ASME for publication in the Journal of Applied Mechanics. Manuscript received October 9, 2014; final manuscript received November 6, 2014; accepted manuscript posted December 12, 2014; published online December 12, 2014. Editor: Yonggang Huang.

 Copyright © 2015 by ASME

Downloaded From: http://appliedmechanics.asmedigitalcollection.asme.org/ on 12/12/2014 Terms of Use: http://asme.org/terms

(Fig. 1, II), and eventually into a helical configuration (Fig. 1, III), which then leads to lock-up of the system with the rod having a vertical helical pitch angle (Fig. 1, IV). Beyond lock-up, no further advancement is possible and the system jams (Fig. 1, V).

Our experimental apparatus comprised a transparent borosilicate glass pipe (2.54 m long) laid horizontally and supported at five equally spaced clamps, into which an elastomeric rod (radius, $r = 1.55$ mm) was inserted using a custom-built injector. The size of the constraint was varied by replacing glass pipes with eight different inner diameters in the range $6.6 < D$ (mm) < 33.6. The combination of rod radius and constraint inner diameter sets the radial clearance, $\Delta r = 1/2(D - 2r)$, as shown in the schematic diagram of the inset of Fig. 2(*a*), varied in the range $1.75 < \Delta r$ (mm) < 15.25. The rod was cast nominally straight (i.e., negligible natural curvature) using a silicone-based rubber (polyvinylsiloxane) with the following material properties: Young's modulus, $E = 1290 \pm 12$ kPa, Poisson's ratio, $\nu \approx 0.5$, and volumetric mass, $\rho = 1200\,\mathrm{kg/m^3}$. Further details of the fabrication protocol of the rod can be found in Refs. [28–30]. The injector was driven by a stepper motor, which allowed for a fine control of the injection speed in the range $1 < v$ (cm/s) < 15. The injector itself was mounted onto a linear air-bearing and connected to a load cell that acquired time series of the injection force, $P(t)$ (t is elapsed experimental time), which was correlated to the injected length, $l(t) = vt$. A representative curve for $P(l)$ is presented in Fig. 1. The configuration of the rod was directly imaged during each test using a digital video camera mounted above the pipe, near the injector.

The constraining pipe was also connected to four electromagnetic shakers (located at midspan between clamps) to provide vertical sinusoidal vibration. Piezoelectric single-axis accelerometers mounted on the pipe, directly above the shakers, were used to characterize the vibration. Both the frequency, f, and amplitude, A, of the sinusoidal driving were recorded, from which the dimensionless acceleration (taken as a control parameter), Γ, was then quantified as

$$\Gamma = 4\pi^2 \frac{Af^2}{g} \tag{1}$$

where g is the acceleration due to gravity. We also define the peak velocity of the sinusoidal vibration, v_{pk}, as

$$v_{\mathrm{pk}} = \frac{\Gamma g}{2\pi f} \tag{2}$$

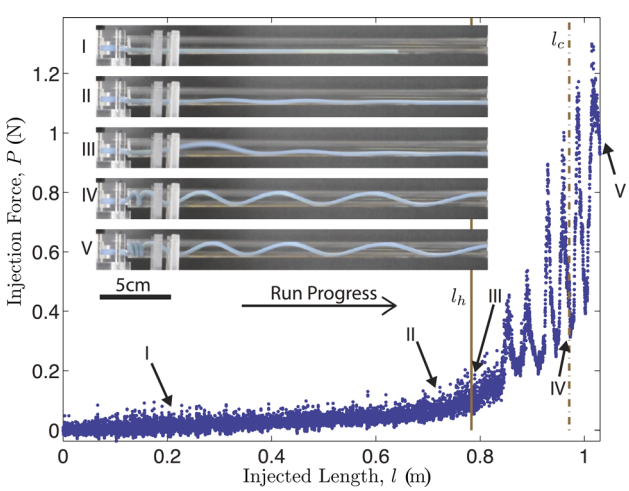

Fig. 1 Injection force, *P*, versus injected length, *l*, for a rod ($E = 1290 \pm 12$ kPa, $\rho = 1200\,\mathrm{kg/m^3}$, and $r = 1.55$ mm) injected into a glass pipe ($D = 12.0$ mm and $\Delta r = 4.4$ mm) at velocity, $v = 0.1$ m/s. Inset: profile-view photographs of configurations at different values of $l = \{0.22, 0.73, 0.79, 0.98, \text{and } 1.05\}$ m. I—straight; II—sinusoidal; III, IV—helix initiation at l_h (solid line) and lock-up at l_c (dashed line); and V—end of test.

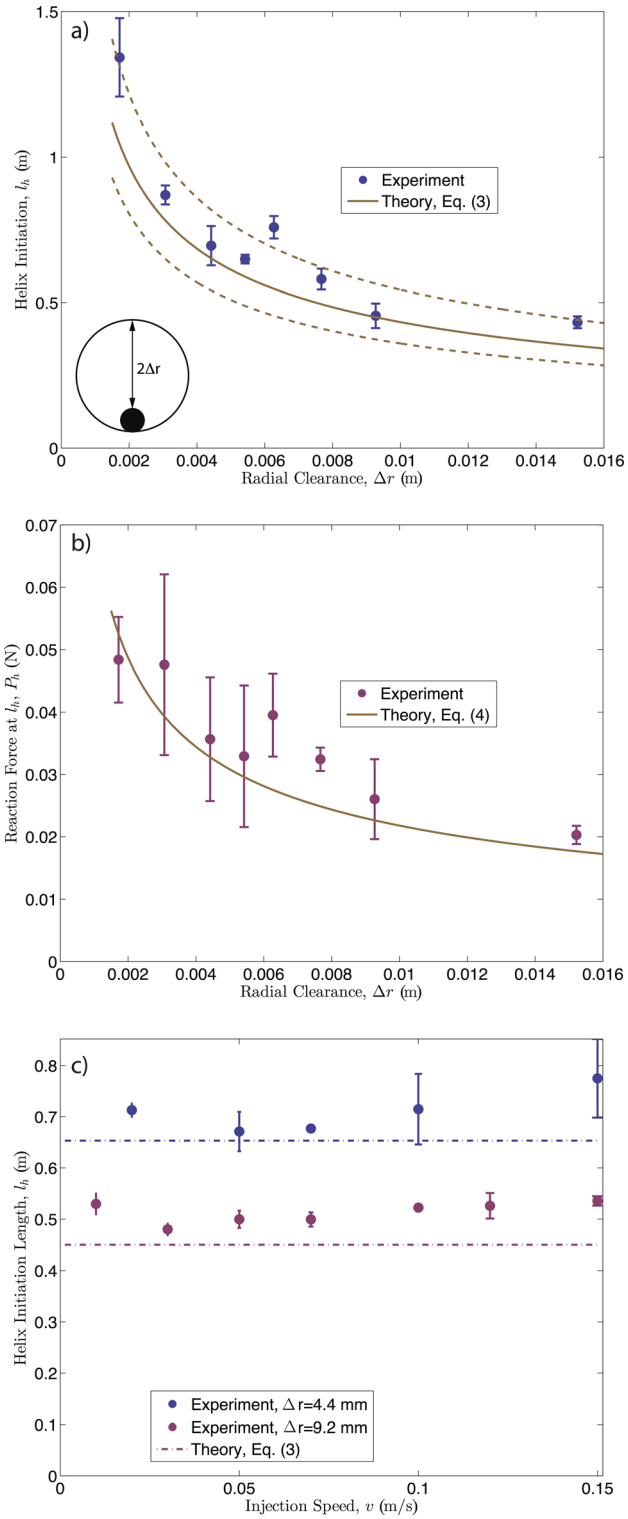

Fig. 2 (*a*) Helix initiation length, l_h, versus radial clearance, Δr. Theoretical prediction comes from Eq. (3), with $\mu = 0.54 \pm 0.11$ (solid line for the mean; dashed lines for the standard deviation). Inset: Schematic definition of Δr. (*b*) Reaction force at helix initiation, P_h, versus Δr. Equation (4) is plotted as a solid line. (*c*) Helix initiation length, l_h, as a function of injection speed, *v*, for two radial clearances, $\Delta r = 4.4$ and 9.2 mm. Dashed lines represent predictions from Eq. (3). For parts (*a*) and (*c*), data points indicate the mean of 10 runs, with error bars representing a standard deviation of 10 runs. For part (*b*), data represents measurements made within 0.02 m of l_h for 10 runs.

Downloaded From: http://appliedmechanics.asmedigitalcollection.asme.org/ on 12/12/2014 Terms of Use: http://asme.org/terms

All tests were performed within the following ranges: Frequency, $35 < f$ (Hz) < 200; amplitude, $0 < A$ (mm) < 0.4; and dimensionless acceleration, $0 < \Gamma < 4$. This oscillatory driving provided a source of energy input into the system and destabilized the frictional contacts between the rod and the pipe. The case when $\Gamma = 0$ is referred to as the *static case* (discussed in Sec. 3) and the *vibrated case* when $\Gamma > 0$ (discussed in Sec. 4). A more detailed account of our experimental apparatus can be found in Ref. [31].

3 Injection Into a Static Pipe

3.1 Experimental Results. We start our investigation in the *static regime* ($\Gamma = 0$). In Fig. 1, we present results of a representative experimental run for the reaction load, P, at the injection point, as a function of total arc length, $l = vt$, of rod injected at a speed of $v = 0.1$ m/s and elapsed time, t. For small values of the injected length (e.g., $l = 0.22$ m, Fig. 1, I), the rod lies along the bottom of the pipe during injection and remains *straight*. We assume that the axial load along the rod increases linearly along its arc length due to frictional resistance with the surface of the pipe. A portion of the rod eventually exceeds the first (of two) buckling load and transitions into a *sinusoidal* configuration. At this point, the rod's geometry is spatially heterogeneous and consists of two segments: A straight portion near the free tip (where the axial load vanishes) and a sinusoidally meandering section nearer the injector (see Fig. 1, II at $l = 0.73$ m) where the axial load is assumed to be maximal and equal to P. During these early stages of injection, the load at the injector, P, scales linearly with l, even as the rod undergoes buckling from the originally straight to the sinusoidal configuration, with no significant increase in resistance to injection. The coefficient of dynamic friction, μ, that characterizes the interaction between the injected rod and the constraining pipe (assuming dry Coulomb friction) was measured from the slope of this linear regime, dP/dl, which yielded $\mu = 0.54 \pm 0.11$, across all constraining pipes and injection speeds tested.

Upon further injection, a second critical buckling load is reached and the rod buckles into a heterogeneous *helical* configuration (Fig. 1, III, $l = l_h = 0.79$ m), with three distinct segments: It is straight near the tip, helical next to the injector and sinusoidal in between. We characterize the onset of helix initiation, l_h, by the total arc length of the injected rod when it first becomes in contact with the top surface of the constraining pipe. Past l_h, the injection force, P, increases sharply with large oscillations that corresponds to the generation of new pitches of the helix. In the helically buckled portion, the normal force between the rod and the pipe also increases dramatically, which leads to *lock-up* (Fig. 1, IV, $l = l_c = 0.98$ m), where the tip of the rod ceases to advance and the length of the helical pitches decreases. Subsequent injection beyond lock-up results in coiling near the injector with self-contact (Fig. 1, V, $l = 1.05$ m). The rod used in our model system was made out of a hyperelastic material, which allowed us to explore this regime of self-contacting helices without undergoing inelastic deformations. However, in most engineering systems, e.g., the metallic coiled tubing mentioned above, such tight curvatures at lock-up would be associated with irreversible failure, such as plasticity or fracture, of the constituent material. On the other hand, the curvatures of the rod up to helix initiation are low and the rod remains in the elastic regime (corresponding to material strains $\sim 1\%$ [8]). As such, for the remainder of our study, we focus on quantifying the injected length of rod, for helix initiation, l_h.

3.2 Comparison With Existing Theories. McCourt et al. [16] and Wicks et al. [17] have previously rationalized the onset of helix initiation through scaling analyses and energy minimization arguments. Both theories consider perfect contact along the entire injected length with *axial* (but no *lateral*) dry Coulomb friction between the rod and the pipe and predict that helix initiation occurs at

$$l_h = \frac{2\sqrt{2}}{\mu}\sqrt{\frac{EI}{w\Delta r}} \tag{3}$$

where EI is the bending stiffness of the rod (I is the second moment of inertia), w is its weight per unit length, and Δr is the radial clearance that characterizes the extent of the cylindrical constraint (see schematic in Fig. 2(*a*), inset). Both groups ported the critical helical buckling load, P_h, from previous studies that analyzed a long fixed length of rod pinned inside a cylinder [10]

$$P_h = 2\sqrt{2}\sqrt{\frac{EIw}{\Delta r}} \tag{4}$$

McCourt et al. [16] also conducted experiments where an elastomeric rod was inserted into glass constraining pipes, obtained injection forces as a function of injected lengths and found good agreement with analytical predictions. Our experiments build on these previous results by systematically controlling the natural curvature of the injected rod (through in-house manufacturing) as well as the friction between the rod and constraining pipe (through a rigorous surface treatment and cleaning protocol). The video recordings of the rod during each experiment, near the injector, also enabled precise tracking of l_h, as shown in the corresponding video frame in Fig. 1, III, which we are able to systematically quantify.

In Fig. 2(*a*), we plot our experimental results for the injected length at helix initiation, l_h, as a function of radial clearance, Δr (the solid data points are means of 10 runs with error bars representing one standard deviation in both directions). The prediction from Eq. (3) is represented by a solid line (for $\mu = 0.54$) and the dashed lines include the uncertainty of the friction measurement in the theoretical result ($\mu = 0.54 \pm 0.11$). In Fig. 2(*b*), we plot the experimentally measured values of the reaction force at helical initiation, P_h. Data points are the mean of 10 runs, with error bars representing one standard deviation in the reaction force over the injected length interval $|l_h - l| < 0.02$m. These experimental data are also compared to the theoretical prediction, Eq. (4), represented by the solid line (no dashed lines are given, as Eq. (4) is independent of μ).

Good agreement is found between experiments and both Eqs. (3) and (4), with no fitting parameters. For example, for tight clearances (e.g., $\Delta r = 1.75 \times 10^{-3}$m), helix initiation occurs significantly later than for larger clearances (e.g., $\Delta r = 9.30 \times 10^{-3}$m), by nearly a factor of three. This can be understood by realizing that for the rod to buckle, it must "climb" the curvature of the constraining pipe, $1/\Delta r$, which carries a greater cost in gravitational potential energy for the smaller diameter pipes.

In Fig. 2(*c*), we plot l_h as a function of injection speed, v, which was not taken into account in the formulations of Eq. (3). We observe that l_h is approximately constant in the range of tested injection speeds ($1 < v$ (cm/s) < 15). This result suggests that inertial effects due to injection can be neglected in this case of zero vertical vibration of the constraint. This is to be contrasted with the results in Sec. 4, for the case of a vertically vibrating the constraining pipe ($\Gamma > 0$), where we find that v can have a significant effect on l_h.

4 Injection Into a Vibrated Pipe

We now turn to strategies to mitigate lock-up. One possibility to delay helix initiation might have been to vary μ, EI, w, or Δr according to Eq. (3), but this is typically impractical for application in the field. Obtaining significant changes in these properties would require replacing the steel used in coiled tubing with more uncommon/costly materials, increasing the thickness of the coiled tubing or pumping additional fluid additives to decrease μ. Instead, we consider transverse vertical vibrations ($\Gamma > 0$) as a driving mechanism to excite dynamic deformation modes in the rod that destabilize the frictional contacts with the constraint. We

Downloaded From: http://appliedmechanics.asmedigitalcollection.asme.org/ on 12/12/2014 Terms of Use: http://asme.org/terms

used high-speed imaging to observe that vertical vibrations of the constraint do indeed cause intermittent contact loss between portions of the rod and the glass pipe.

Next, we systematically study the dependence of helix initiation during vibration tests on injection speed (Sec. 4.1), dimensionless acceleration (Sec. 4.2), and frequency of vibrations (Sec. 4.3). The static helix initiation length, l_h, for the *static case* described above is taken as a reference base, against which improvements are compared to. As such, for the remainder of this paper, values of helix initiation length for the *vibrated case* will be normalized by l_h, for the same radial clearance, and reported as $\bar{l}_h$. Due to the agitation of the rod/constraint contact due to the vibration, five tests were run for each experimental data point plotted (instead of the ten for static case), with error bars representing the standard deviation.

4.1 The Effect of Injection Speed. In Fig. 3, we plot the experimentally measured normalized helix initiation length, $\bar{l}_h$, as a function of the normalized injection speed, $\bar{v} = v/v_{pk}$, where v_{pk} is the peak velocity of the sinusoidal driving, defined in Eq. (2). In this experimental run, we used a pipe with diameter $D = 21.7$ mm, resulting in a radial clearance $\Delta r = 9.3$ mm. The two horizontal dashed lines at $\bar{l}_h \approx 1$ correspond to the range of experimental values measured in the static case, shown above in Fig. 2(*c*). Three data sets are shown for different vibration frequencies, $f = \{50, 100, \text{and } 200\}$ Hz, while keeping the dimensionless acceleration constant at $\Gamma = 2$. Two distinct regimes can be identified, which are separated by the vertical line in the plot.

For $\bar{v} > 1$, which we refer to as the *fast* injection speed regime, the improvements in $\bar{l}_h$ are small (less than an improvement factor of 1.5 above the static value) and independent of *f*. By contrast, in the *slow* injection speed regime, for $\bar{v} < 1$, the helix initiation length increases dramatically with decreasing $\bar{v}$ and improvements of up to a factor of three are observed. Moreover, these improvements are largest for the lowest tested frequency, $f = 50$ Hz. We have not yet been able to rationalize this frequency effect but hope that our results will motivate future work in this direction. For experiments with tighter clearances (e.g., with $D = 12.0$ mm, $\Delta r = 4.4$ mm), we have observed similar improvements in $\bar{l}_h$, for $\bar{v} < 1$.

The behavior in the slow injection regime is in contrast to the results of the static case shown in Fig. 2(*c*), which were independent of *v*. We speculate that, under vibrations of the constraining pipe, the velocity-dependent behavior arises from the introduction of a new time-scale. This is presumably associated with the dynamics of relaxation of a sinusoidally buckled rod into a straight configuration, under destabilization of the frictional contacts caused by vertical vibration. Though we have not yet been able to quantitatively rationalize this effect, our results point to the existence of a critical injection speed, below which reach can be dramatically improved for a given energy input through the vibration loading.

4.2 The Effect of Dimensionless Acceleration. We proceed by studying the effect of varying the dimensionless acceleration, Γ, of the imposed vibration, while fixing the injection speed at $v = 0.1$ m/s, in the fast injection regime ($1.6 < \bar{v} < 62.5$ for all cases tested). In Fig. 4, we plot $\bar{l}_h$ as a function of Γ, for three values of vibration frequencies, $f = \{50, 100, \text{and } 200\}$ Hz. All three datasets exhibit approximately the same behavior and there is minimal dependence on frequency (similarly to what was observed in Fig. 3, for $\bar{v} > 1$). For low values of acceleration, in the range $0 < \Gamma < 1$, we find that $\bar{l}_h \sim 1$. Beyond $\Gamma > 1$, however, there is a monotonic increase of $\bar{l}_h$. These results provide a minimum design requirement for the magnitude of acceleration needed to induce improvements in reach.

Using high-speed video, the flight time of the rod, i.e., the time during which a section of the rod loses contact with the surface of the vibrating pipe, was also found to increase monotonically with increasing Γ. This partial and intermittent reduction in contact is responsible for a reduction of the axial stresses along the rod, which in turn results in an increase in $\bar{l}_h$.

4.3 The Effect of Frequency. In Fig. 5, we present the frequency dependence of $\bar{l}_h$, for datasets with different values of the radial clearance, Δr, in the slow injection regime, $\bar{v} = 0.1$. Throughout, the acceleration was kept constant at $\Gamma = 1.75$. The frequency response of the system can be classified under two general groups, with qualitatively different behavior. For some values of radial clearance (e.g., $\Delta r = \{1.75, 6.6, \text{and } 7.7\}$ mm, data points connected with dashed lines), $\bar{l}_h$ is approximately constant or slightly decreasing with increasing *f*. The curves for the remaining

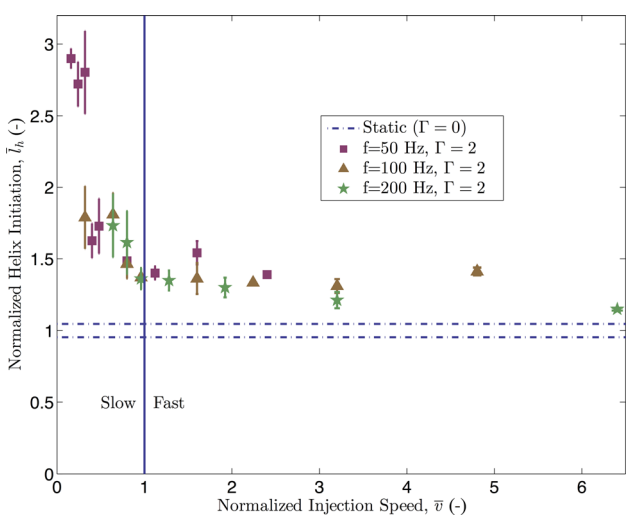

Fig. 3 Normalized helical initiation length, $\bar{l}_h$, versus normalized injection speed, $\bar{v}$, for a rod injected into a pipe with $D = 21.7$ mm and $\Delta r = 9.3$ mm. Experimental error bars are the standard deviations of 5 runs per injection speed. The dimensionless acceleration is $\Gamma = 2$, with $f = \{50, 100, \text{and } 200\}$ Hz. The dashed horizontal lines represent the range of the experiments with no vibration reported in Fig. 2(*c*), and the solid vertical line shows the separation between *fast* ($\bar{v} > 1$) and *slow* ($\bar{v} < 1$) injection speeds.

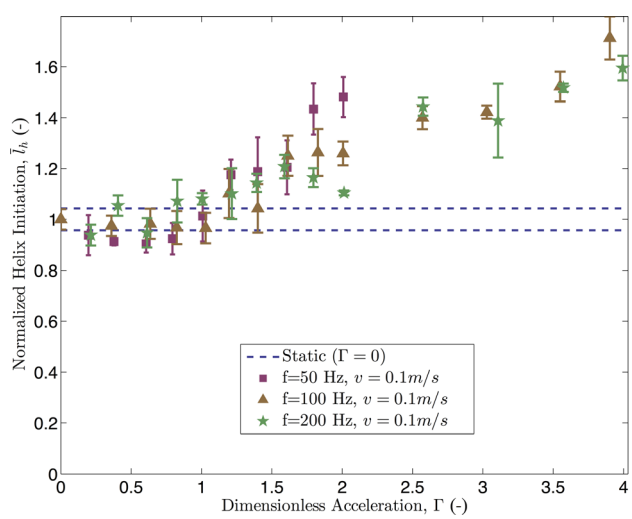

Fig. 4 Normalized helical initiation length, $\bar{l}_h$, versus dimensionless acceleration, Γ, for a rod injected into a pipe with $D = 21.7$ mm and $\Delta r = 9.3$ mm. The error bars on the experimental data are the standard deviations of 5 runs per injection speed. For all runs, the injection speed was $v = 0.1$ m/s (*fast* injection speed for all cases) and three vibration frequencies were tested, $f = \{50, 100, \text{and } 200\}$ Hz. The dashed lines represent the range of the experiments with no vibration reported in Fig. 2(*c*).

Downloaded From: http://appliedmechanics.asmedigitalcollection.asme.org/ on 12/12/2014 Terms of Use: http://asme.org/terms

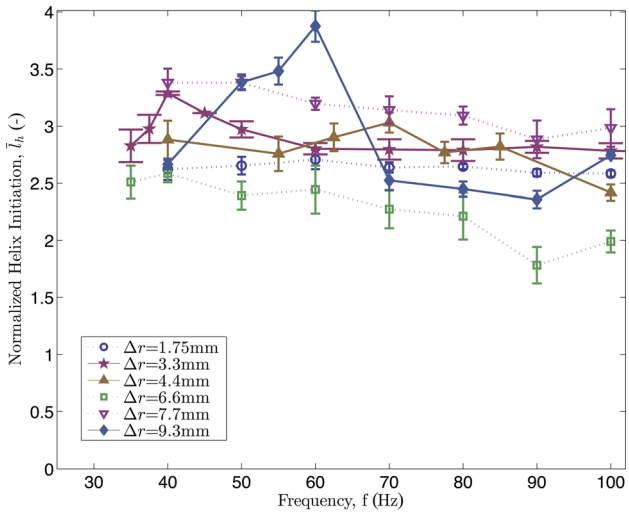

Fig. 5 Normalized helix initiation length, $\bar{l}_h$, versus vibration frequency, *f*, for glass pipes with different radial clearances (see legend), at $\Gamma = 1.75$ and $\bar{v} = 0.1$. Solid lines indicate radial clearances exhibiting resonant peaks ($\Delta r = \{3.2, 4.4, \text{and } 9.3\}$ mm), while dashed lines indicate radial clearances which exhibit no such peaks ($\Delta r = \{1.75, 6.6, \text{and } 7.7\}$ mm).

clearances ($\Delta r = 3.3$, 4.4, and 9.3 mm, data points connected with solid lines) exhibit peak responses at specific values of $f \approx 40$, 60, and 70 Hz, respectively, reminiscent of a resonance behavior. The largest clearance, $\Delta r = 9.3$ mm, shows the strongest frequency dependence, with its peak response leading to $\bar{l}_h$ varying between a factor of improvement between 2.5 and 4. Other clearances (both with and without peak responses) exhibit improvements of a factor typically between 2.5 and 3.5. For the smaller clearances ($\Delta r = \{1.75, 3.3\}$ mm), the experimental apparatus was extended to 3.65 m, maintaining the same clamp and shaker spacing, to accommodate these gains in l_h.

For the clearances with a peak response, the peaks are observed at frequencies equivalent to the resonance of a clamped beam with a length equal to a fraction of the predicted buckled wavelength (between one-quarter and one-half of the buckled wavelength). High-speed video analysis also indicates that the rod loses contact with the bottom of the constraint between the peaks of the sinusoidally buckled rod, which is equivalent to approximately a half-wavelength length scale. The nontrivial dependence of the frequency at which these peaks occur on Δr is likely complicated by the loss of contact that arises from the incompatibility between the curvatures of the buckled configuration of the rod and the radius of the constraining pipe. A detailed analysis of this effect would require a predictive numerical analysis of the statistics of the segments of the buckled wavelength that remain in contact with the pipe, which is beyond the scope of this experimental work.

Finally, we note that while keeping Γ constant for ease of comparison to Secs. 4.1 and 4.2, the power supplied to the model system through the shakers was frequency dependent. Specifically, the power supplied at constant Γ is inversely proportional to vibration frequency (that is, Power $\propto \Gamma v_{pk} \propto 1/f$). While this is in line with the observed trend of decreasing l_h with increasing f for the clearances without peak responses, it may also mask other frequency-dependent processes, such as a peak response behavior. However, our finding that there are no *deconstructive* frequency ranges (that would lead to $\bar{l}_h < 1$) is important for practical engineering applications to extend reach, as it demonstrates that there are no detrimental frequencies of vibration.

5 Conclusion

We reported results form an experiment on the injection of an elastic rod into a horizontal, cylindrical constraint. Initial tests of the so-called static configuration (with no vertical vibration of the constraining pipe) showed good agreement with existing theory regarding the length of rod and the reaction force at helical initiation, both of which were found to be independent of the speed of injection. Upon vertical vibration of the constraint, however, we found that helix initiation could be delayed, thereby extending horizontal reach up to a factor of four when compared to the static case. This extension in reach is a result of the loss of contact between the injected rod and the constraint.

In the vibrated case, both the injection speed (provided $\bar{v} < 1$) and the magnitude of the acceleration (for $\Gamma > 1$) have a strong effect on determining the magnitude of this reach extension. At slow injection speeds, frequency was observed to have a complex effect on reach extension, with some clearances observed to exhibit resonant peaks, while others did not. We proposed that the frequency at which these peaks occur is set by the mechanical resonance of portions of the rod that lose contact with the constraint, although further investigation will required for a predictive understanding of this phenomena. This nontrivial effect presumably arises from the incompatibility between the curvature of the rod in its buckled configuration and the radius of the cylindrical constraint, which affects the contact ratio between the two.

We hope that our experimental results will motivate future computational and analytical efforts toward rationalizing this new active mechanism to inject a rod farther into a cylindrical constraint, which is a problem of practical engineering relevance across several length scales. Whereas, for convenience, we have focused on the case of a vibrated constraint, we speculate that similar performances should be realizable by vibrating the rod instead.

Acknowledgment

We thank Katia Bertoldi and Tianxiang Su for helpful discussions. The authors are grateful for financial support from Schlumberger and the National Science Foundation (CMMI-1129894), as well as The Modal Shop for support involving their SmartShaker technology.

References

[1] van Adrichem, W., and Newman, K., 1993, "Validation of Coiled-Tubing Penetration Predictions in Horizontal Wells," J. Pet. Technol., **45**(2), pp. 155–159.
[2] Svenšek, D., and Podgornik, R., 2008, "Confined Nanorods: Jamming due to Helical Buckling," Phys. Rev. E, **77**(3), p. 031808.
[3] Bassett, E. K., Slocum, A. H., Masiakos, P. T., Pryor, H. I., Farokhzad, O. C., and Karp, J. M., 2009, "Design of a Mechanical Clutch-Based Needle-Insertion Device," Proc. Natl. Acad. Sci., **106**(14), pp. 5540–5545.
[4] Mitchell, R. F., 2008, "Tubing Buckling—The State of the Art," SPE Drill. Completion, **23**(4), pp. 361–370.
[5] McCourt, I., Truslove, T., and Kubie, J., 2002, "Penetration of Tubulars Into Horizontal Oil Wells," Proc. Inst. Mech. Eng., Part C, **216**(12), pp. 1237–1245.
[6] Tailby, R., Cobb, D., Riva, M., Jones, C., Rydland, J., and Christensen, O., 1993, "A Joint Industry Research Project to Investigate Coiled-Tubing Buckling," Offshore Europe, pp. 993–1002.
[7] Lubinski, A., 1950, "A Study of the Buckling of Rotary Drilling Strings," Drilling and Production Practice, pp. 178–214.
[8] Lubinski, A., and Althouse, W., 1962, "Helical Buckling of Tubing Sealed in Packers," J. Pet. Technol., **14**(6), pp. 655–670.
[9] Cheatham, J., Jr., 1984, "Helical Postbuckling Configuration of a Weightless Column Under the Action of Axial Load," SPE J., **24**(4), pp. 467–472.
[10] Chen, Y., Lin, Y., and Cheatham, J., 1990, "Tubing and Casing Buckling in Horizontal Wells (Includes Associated Papers 21257 and 21308)," J. Pet. Technol., **42**(2), pp. 140–141.
[11] Mitchell, R., 1986, "Simple Frictional Analysis of Helical Buckling of Tubing," SPE Drill. Eng., **1**(6), pp. 457–465.
[12] Wu, J., and Juvkam-Wold, H., 1993, "Study of Helical Buckling of Pipes in Horizontal Wells," SPE Production Operations Symposium, pp. 867–876.
[13] Gao, G., and Miska, S., 2009, "Effects of Boundary Conditions and Friction on Static Buckling of Pipe in a Horizontal Well," SPE J., **14**(4), pp. 782–796.
[14] Gao, G., and Miska, S., 2010, "Effects of Friction on Post-Buckling Behavior and Axial Load Transfer in a Horizontal Well," SPE J., **15**(4), pp. 1104–1118.
[15] Suryanarayana, P., and McCann, R., 1994, "Experimental Study of Buckling and Post-Buckling of Laterally Constrained Rods: Part 1—Frictional Effects," ASME Energy-Source Technology Conference and Exhibition, New Orleans, LA, Jan. 23–26, pp. 23–27.
[16] McCourt, I., Truslove, T., and Kubie, J., 2004, "On the Penetration of Tubular Drill Pipes in Horizontal Oil Wells," Proc. Inst. Mech. Eng., Part C, **218**(9), pp. 1063–1081.

Downloaded From: http://appliedmechanics.asmedigitalcollection.asme.org/ on 12/12/2014 Terms of Use: http://asme.org/terms

[17] Wicks, N., Wardle, B., and Pafitis, D., 2008, "Horizontal Cylinder-in-Cylinder Buckling Under Compression and Torsion: Review and Application to Composite Drill Pipe," Int. J. Mech. Sci., **50**(3), pp. 538–549.
[18] Acock, A., ORourke, T., Shirmboh, D., Alexander, J., Andersen, G., Kaneko, T., Venkitaraman, A., López-de Cárdenas, J., Nishi, M., Numasawa, M., Yoshioka, K., Roy, A., Wilson, A., and Twynam, A., 2004, "Practical Approaches to Sand Management," Oilfield Rev., **16**(1), pp. 10–27.
[19] Afghoul, A., Amaravadi, S., Boumali, A., Calmeto, J., Lima, J., Lovell, J., Tinkham, S., Zemlak, K., and Staal, T., 1994, "Coiled Tubing: The Next Generation," Oilfield Rev., **6**(4), pp. 9–23.
[20] Bennetzen, B., Fuller, J., Isevcan, E., Krepp, T., Meehan, R., Mohammed, N., Poupeau, J.-F., and Sonowal, K., 2010, "Extended-Reach Wells," Oilfield Rev., **22**(3), pp. 4–15.
[21] Summers, T., Larsen, H. A., Redway, M., and Hill, G., 1995, "The Use of Coiled Tubing During the Wytch Farm Extended Reach Drilling Project," International Meeting on Petroleum Engineering, pp. 23–36.
[22] McCourt, I., and Kubie, J., 2005, "Limits on the Penetration of Coiled Tubing in Horizontal Oil Wells: Effect of the Pipe Geometry," Proc. Inst. Mech. Eng., Part C, **219**(11), pp. 1191–1197.
[23] Zheng, A., and Sarmad, A., 2005, "The Penetration of Coiled Tubing With Residual Bend in Extended-Reach Wells," SPE Annual Technical Conference and Exhibition, Dallas, TX, Oct. 9–12, pp. 220–225.
[24] Bhalla, K., 1995, "Coiled Tubing Extended Reach Technology," Offshore Europe Conference, Aberdeen, UK, Sept. 5–8, pp. 392–405.
[25] Al Shehri, A., Al-Driweesh, S., Al Omari, M., and Al Sarakbi, S., 2007, "Case History: Application of Coiled Tubing Tractor to Acid Stimulate Open Hole Extended Reach Power Water Injector Well," SPE Asia Pacific Oil and Gas Conference, Jakarta, Indonesia , Oct. 30–Nov. 1, pp. 989–996.
[26] Al-Buali, M. H., Dashash, A. A., Shawly, A. S., Al-Guraini, W. K., Al-Driweesh, S. M., Bugrov, V., and Nicoll, S., 2009, "Maximizing Coiled Tubing Reach During Logging of Extended Horizontal Wells Using E-Line Agitator," Kuwait International Petroleum Conference and Exhibition, Kuwait City, Kuwait, Dec. 14-16, pp. 324–334.
[27] Audoly, B., and Pomeau, Y., 2010, *Elasticity and Geometry: From Hair Curls to the Non-Linear Response of Shells*, Oxford University Press, New York.
[28] Lazarus, A., Miller, J. T., and Reis, P. M., 2013, "Continuation of Equilibria and Stability of Slender Elastic Rods Using an Asymptotic Numerical Method," J. Mech. Phys. Solids, **61**(8), pp. 1712–1736.
[29] Lazarus, A., Miller, J. T., Metlitz, M., and Reis, P. M., 2013, "Contorting a Heavy and Naturally Curved Elastic Rod," Soft Matter, **9**(34), pp. 8274–8281.
[30] Miller, J. T., Lazarus, A., Audoly, B., and Reis, P. M., 2014, "Shapes of a Suspended Curly Hair," Phys. Rev. Lett., **112**(6), p. 068103.
[31] Miller, J. T., 2014, "Mechanical Behavior of Elastic Rods Under Constraint," Ph.D. thesis, Massachusetts Institute of Technology, Cambridge, MA.

Downloaded From: http://appliedmechanics.asmedigitalcollection.asme.org/ on 12/12/2014 Terms of Use: http://asme.org/terms